J Fluoresc (2007) 17:759–765
DOI 10.1007/s10895-007-0187-z

Detection and Analysis of Protein Aggregation with Confocal Single Molecule Fluorescence Spectroscopy

Frank Hillger · Daniel Nettels · Simone Dorsch · Benjamin Schuler

Received: 16 February 2007 / Accepted: 19 March 2007 / Published online: 20 April 2007

Abstract The misfolding and aggregation of proteins is a common phenomenon both in the cell, in *in vitro* protein refolding, and the corresponding biotechnological applications. Most importantly, it is involved in a wide range of diseases, including some of the most prevalent neurodegenerative disorders. However, the range of methods available to analyze this highly heterogeneous process and the resulting aggregate structures has been very limited. Here we present an approach that uses confocal single molecule detection of FRET-labeled samples employing four detection channels to obtain information about diffusivity, anisotropy, fluorescence lifetimes and Förster transfer efficiencies from a single measurement. By combining these observables, this method allows the separation of subpopulations of folded and misfolded proteins in solution with high sensitivity and a differentiation of aggregates generated under different conditions. We demonstrate the versatility of the method with experiments on rhodanese, an aggregation-prone two-domain protein.

Keywords Protein aggregation · Protein folding · Protein misfolding · Amyloid · Multiparameter fluorescence detection · Single molecule fluorescence spectroscopy · Förster resonance energy transfer

F. Hillger · D. Nettels · S. Dorsch · B. Schuler (✉)
Biochemisches Institut, Universität Zürich,
Winterthurerstr. 190, 8057 Zurich, Switzerland
e-mail: schuler@bioc.uzh.ch

Introduction

The misassembly of protein molecules into non-functional aggregates has been a well-known phenomenon for about a century (for a review, see [1]). However, for a long time "there was little interest in the serious study of the phenomena of aggregation" [2], because they were considered artificial side-reactions irrelevant for the study of protein folding and assembly. This point of view changed with the advent of biotechnology and recombinant protein expression, and especially the discovery of molecular diseases connected to protein misassembly. In biotechnology, the expression of large concentrations of heterologous proteins often leads to the formation of intracellular "inclusion bodies," large agglomerates of misfolded proteins, which then need to be solubilized and refolded to obtain functional, soluble protein [3]. Even more important was the realization that a large number of human pathologies involve the misfolding of proteins [4], showing that aggregation is a physiologically relevant process that competes with productive protein folding reactions. Such amyloidoses involve a wide range of diseases, the most well-known of which are neurodegenerative disorders such as Alzheimer's disease or the prion diseases.

This new perspective has stimulated huge interest in the structure of aggregates and the mechanisms of their formation. But even though significant advances have been made over the past decades in both aspects [5–8], most aggregation reactions have proven exceedingly difficult to study experimentally. Some of the fundamental underlying difficulties are the large heterogeneity of structures formed, the high reaction orders of such multimolecular processes, and the exquisite sensitivity to solution conditions, to name but a few. The large number of parameters required to define the corresponding mechanisms is in stark contrast to

the methods typically used to follow aggregation reactions; the most common techniques include static light scattering and assays involving aggregate-sensitive fluorescent dyes, such as thioflavin T [9]. Such measurements usually only provide a single observable like fluorescence or scattering intensity, e.g. as a function of time in kinetic studies, averaged over the entire population of particles in the solution, ranging from monomeric proteins to small oligomers and large aggregates. Correspondingly, there is a large interest in new approaches to investigate these heterogeneous systems.

An obvious advantage would be the direct imaging of individual particles in the reaction, and a couple of methods already provide this possibility. Atomic force microscopy and fluorescence imaging, for instance, have been used to follow amyloid formation on the level of individual fibrils [10, 11]. However, these experiments are limited to reactions occurring on surfaces, which are well known to influence aggregation. The resulting observations can thus usually not be transferred to aggregation processes in free solution. Electron microscopy and cryo-electron microscopy also provide the possibility to image individual particles, but the indispensable sample fixation allows only a snapshot of the situation in solution. The most powerful methods for assessing the heterogeneity of oligomeric molecular species in solution have been dynamic light scattering [12–14] and fluorescence correlation spectroscopy (FCS) [15–19]. In both cases, the heterogeneity of particles diffusing through a laser beam results in a distribution of diffusion coefficients, which in favorable cases can be translated into a distribution of particle sizes [16, 19], and can even be analyzed kinetically [14]. An example of such a measurement is shown in Fig. 2 for the aggregation of the two-domain protein rhodanese (Fig. 1), a paradigm for protein misassembly [20, 21]. Whereas the monomeric protein exhibits a correlation function that can be well described with a single diffusion coefficient, samples with aggregates present exhibit broad distributions of diffusion times. Once the majority of protein molecules is present in aggregates, the signal is dominated by species with very large diffusion coefficients (Fig. 2). The strong signal from larger aggregates results in an exquisite sensitivity for the early stages of assembly [16], but the available information is limited to the diffusivity of the particles. Here we present an approach to increase the number of observables by using confocal single molecule spectroscopy with four detection channels and pulsed excitation on samples suitably labeled for Förster resonance energy transfer (FRET). By identifying fluorescence bursts from individual molecules or assemblies, this methodology provides access to the fluorescence intensities, lifetimes, anisotropies and distances within individual particles [22] and allows a direct separation of folded and misfolded subpopulations, analogous to the separation of folded and unfolded subpopulations in the folding of small, highly soluble proteins [23–26].

Materials and methods

Synthesis and labeling of rhodanese

Cysteine residues were introduced by site-directed mutagenesis at positions 135 and 174, respectively, replacing two lysine residues of the wild-type protein. The cysteine variant of rhodanese was purified as described for the wild-type protein [27]. Labeling was carried out according to the procedures supplied by the manufacturer (Molecular Probes/Invitrogen) utilizing maleimide-thiol chemistry. A two-fold molar excess of Alexa Flour 488 and Alexa Flour 594 maleimide derivatives were added to the protein. After 1 h of incubation at room temperature, unreacted dye was removed by gel filtration. The labeling efficiency as determined from chromatograms was nearly 100%. Sodium

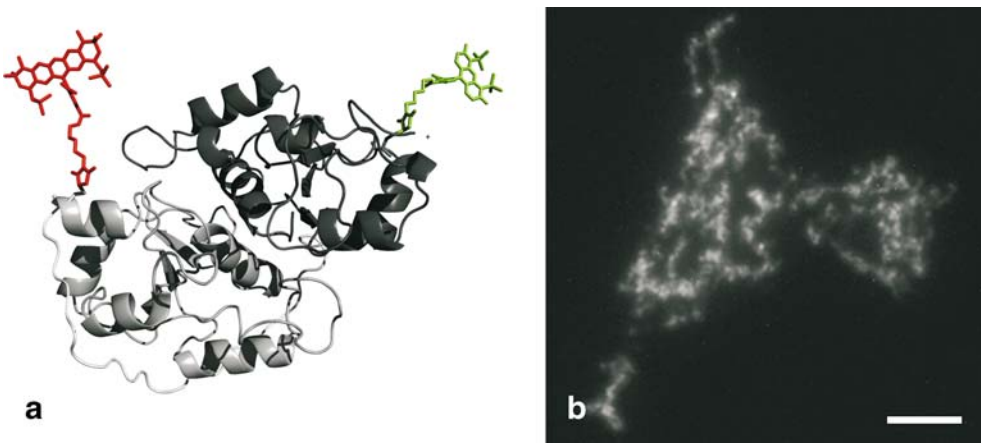

Fig. 1 **a** Cartoon of rhodanese K135C-K174C (model based on the wild type crystal structure [32]) with Alexa Flour 488 maleimide and Alexa Flour 594 maleimide, respectively, coupled to the two cysteine residues introduced via site-directed mutagenesis. (Chromophores placed manually in arbitrary orientation, figure created with PyMOL [38].) **b** Total internal reflection fluorescence microscopy image of a large aggregate from donor-only labeled rhodanese (scale bar: 5 μm)

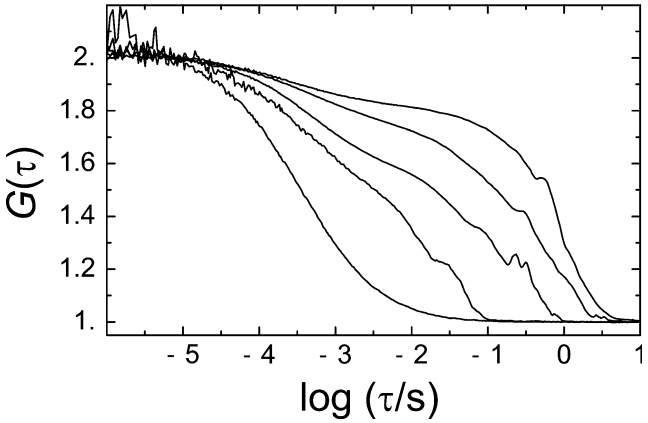

Fig. 2 Fluorescence correlation spectroscopy (FCS) analysis of data from samples containing aggregates of rhodanese prepared under different conditions, resulting in increasing degrees of aggregation (*from left to right*). Correlation functions were calculated from the donor fluorescence signal in cross correlation mode to avoid the influence of detector afterpulsing, and the amplitude was normalized to 1 at τ=10 μs. Detailed description and analysis for the samples represented by the FCS curves four and five (*from left*) are given in the results section and the legends to Figs. 3 and 5, respectively

thiosulfate was removed from the active site of rhodanese by reaction with potassium cyanide and subsequent gel filtration to prevent chemical side reactions due to free-radical formation after unfolding.

Sample preparation

Samples of labeled rhodanese were mixed with unlabeled wild-type rhodanese at molar ratios between 1:100 and 1:10,000. Aggregation was triggered either by elevated temperature or by dilution from GdmCl-containing solutions into native buffer conditions, and was stopped by cooling and/or further dilution after different incubation times. Samples were measured in 100 mM potassium phosphate buffer, 200 mM mercaptoethanol and 1 mM EDTA, adjusted to pH 7.0. 0.001% Tween 20 (Pierce, Rockford, IL) were added to prevent surface adhesion of the protein [25]. Chemical unfolding was done in the same buffer containing appropriate amounts of GdmCl (Pierce, Rockford, IL). Data were recorded for 30–120 min.

Confocal fluorescence spectroscopy

Observations of single-molecule fluorescence were made using a MicroTime 200 confocal microscope (PicoQuant, Berlin, Germany) equipped with a 470 nm pulsed diode laser (LDH 470) operated at 40 MHz (average power 130 μW), an Olympus UplanApo 60×/1.20 W objective, and four detection channels (PerkinElmer Optoelectronics SPCM-AQR-15 avalanche photodiodes). Sample fluorescence was first separated by a polarizing beam splitter cube, and then (for each polarization) split into donor and acceptor components using dichroic mirrors (Chroma 585DCXR), and two final filters (Chroma HQ525/50, Omega 600ALP). Each component was focused onto an avalanche photodiode, and the arrival time of every detected photon was recorded relative to the exciting laser pulse with a time resolution of 38 ps using a TimeHarp PC card (PicoQuant).

Single molecule data reduction and analysis

Successive photons detected in any channel separated by less than 100 μs were combined into one burst. A burst was retained as a significant event if the total number of counts exceeded 50. Identified bursts were corrected for background, differences in quantum yields, the different collection efficiencies of the detection channels, cross-talk (acceptor emission detected in the donor channel and donor emission detected in the acceptor channel), and direct excitation of the acceptor with the matrix approach described previously [25, 28]. Fluorescence anisotropies r were additionally corrected for effects due to the large numerical aperture of the objective as described by Koshioka et al. [29]:

$$r = \frac{n_x - n_y}{(1 - 3l_2)n_x + (2 - 3l_1)n_y},$$

where n_x and n_y are the photon counts detected in the orientation parallel and perpendicular to the polarization of the exciting laser light, respectively (corrected as described above [25, 28]), and l_1 and l_2 are the correction factors. We found l_1 and l_2 to be 0.227 and 0.059 for the configuration of the instrument used here. Fluorescence lifetimes were estimated from individual bursts with a maximum likelihood algorithm [28, 30]. The dependence of the Förster radius R_0 on denaturant concentration was determined by measuring changes in spectral overlap, donor quantum yield, and the refractive index of the solvent, and was found to be dominated by the change in refractive index [28].

Results and discussion

Figure 1 illustrates the molecule under study, bovine liver rhodanese. This protein has been used in a wide range of protein folding and misfolding experiments [20, 21] and—due to its strong aggregation tendency and corresponding reluctance to refold to the native state *in vitro*—has been a favorite object for the investigation of molecular chaperones, proteins that assist protein folding in vivo [31]. At positions 135 and 174, where cysteine residues were introduced by site-directed mutagenesis, we labeled the protein with donor and acceptor fluorophores (Alexa 488 and 594) that form a FRET pair with a Förster radius R_0 of

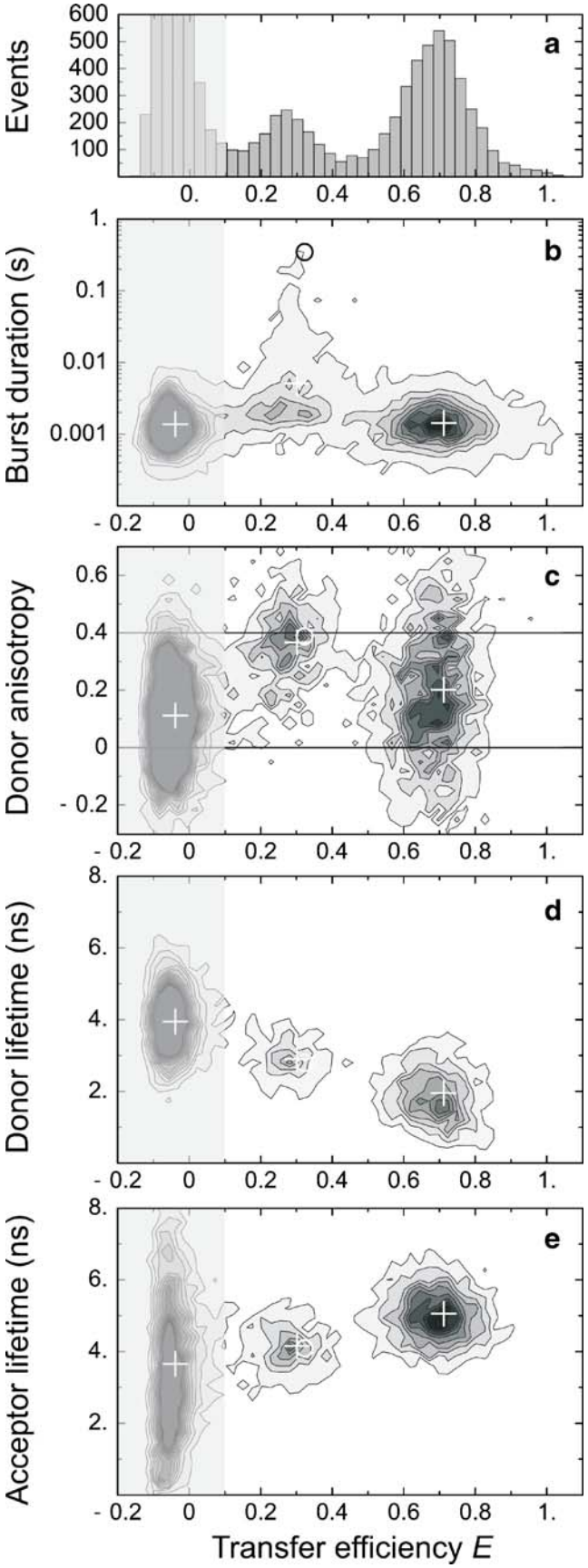

about 54 Å [26, 28]. Figure 1b shows total internal reflection fluorescence microscopy images of aggregated rhodanese labeled only with donor dye, indicating that rhodanese forms filamentous oligomers that associate into more irregular superstructures.

In a typical experiment, a mixture of doubly labeled and unlabeled rhodanese was unfolded in the denaturant guanidinium chloride (GdmCl) and then—by rapid dilution into a suitable buffer—transferred to conditions favoring folding. Samples were then analyzed using confocal single molecule spectroscopy, where the fluorescence light was first separated by polarization, and for each polarization again into donor and acceptor emission, using four detection channels total. Bursts of fluorescence originating from single particles diffusing through the confocal volume were identified and analyzed individually in terms of fluorescence intensity, transfer efficiency, fluorescence lifetime, steady-state anisotropy, and burst duration (see "Materials and methods"), from which one- or two-dimensional histograms were generated.

In mixtures containing suitably chosen concentrations of labeled and unlabeled protein, part of the protein was found to fold to the native state, resulting in a FRET efficiency E of about 0.70 in a transfer efficiency histogram calculated from the numbers of donor and acceptor photons in every burst (Fig. 3a) [25], as expected from the intramolecular distance according to the crystal structure of the protein [32]. However, a second population at lower apparent transfer efficiencies was observed, and corresponds to protein aggregates, as explained in detail below. (The third peak at transfer efficiencies close to zero is due to molecules labeled only with donor.) This partitioning between folding and aggregation is a characteristic of virtually all protein misfolding reactions and is typically found to be highly concentration-dependent because of the high reaction order of aggregation [1]. Correspondingly, the ratio between folded and aggregated molecules observed in our experiments also depended strongly on the total protein concentration (data not shown). Figure 3a illustrates one of

◀**Fig. 3** Multiparameter fluorescence detection analysis of rhodanese aggregates in the presence of native protein. The sample was prepared by refolding a 1:100 mixture of labeled and unlabeled rhodanese after unfolding in 4 M GdmCl. The unfolded material was diluted 10-fold into buffer without GdmCl. After 3 minutes the sample was further diluted to a total nominal protein concentration of 50 nM. Data were recorded for 120 minutes (see "Materials and methods"). **a** FRET efficiency histogram. The shaded region close to a transfer efficiency of zero originates from molecules without an acceptor dye [39]. **b**–**d** Contour plots of two-dimensional histograms calculated from different parameters versus transfer efficiency. *White crosses* mark the respective average values for every subpopulation. The *circles* mark the location of the single burst shown in detail in Fig. 4. The *horizontal lines* in **c** indicate the maximum possible range of the fluorescence anisotropy (0 to 0.4)

the key advantages of this experimental approach: native and misfolded subpopulations can be separated and investigated independently. For example, in experiments done under a wide range of conditions, we found the transfer efficiency of the folded fraction to be invariant and independent of the apparent transfer efficiency of the aggregates. The properties of the aggregates, however, turned out to be more variable and dependent on the solution conditions used to generate them (see below). In all experiments, the ratio of labeled to unlabeled protein is sufficiently low such that intermolecular transfer can be excluded even within aggregates.

Clear evidence for aggregates being the origin of the peak at <E> = 0.28 in the transfer efficiency histogram comes from the durations of the corresponding fluorescence bursts and the resulting anisotropies. Figure 3b shows a two-dimensional histogram of burst duration (on a logarithmic scale) versus transfer efficiency for the same data set as in Fig. 3a. As expected from the FCS data (Fig. 2), the burst durations are strongly increased for the aggregates, but in this multiparameter analysis, we can explicitly separate the folded and aggregated subpopulations. A large range of burst durations is found for the aggregates, suggesting a broad range of particle sizes, with the longest bursts approaching times of one second. Note, however, that the burst durations cannot be used directly to calculate diffusion coefficients, because in contrast to FCS data, only large bursts are selected for this analysis. Part of a corresponding fluorescence trajectory is given in Fig. 4a, illustrating the presence of very large bursts. A representative large burst assigned to a single aggregate particle with a duration of ~0.3 s (circles in Fig. 3b–e) is shown in more detail in Fig. 4b. The high count rates from these very large aggregates suggest the presence of several fluorophores per aggregate, in spite of the large ratio of unlabelled to labeled rhodanese molecules present in the sample.

Figure 3c shows the histogram of donor anisotropy r versus transfer efficiency. While the mean value $\langle r \rangle \approx 0.18$ for natively folded rhodanese molecules, the value for the aggregates is about 0.35, indicating significantly lower rotational mobility of the donor chromophore. Assuming parallel absorption and emission dipoles of the chromophore, and taking into account the respective donor fluorescence lifetimes (Fig. 3d), these anisotropies result in an average rotational correlation time τ_c of ~1.5 ns for the folded subpopulation. This value is higher than the value for the free dye (~200 ps [33]), but significantly lower than the rotational correlation time expected for a globular protein the size of rhodanese (~13 ns [34]), suggesting that the chromophore is rather mobile on the surface of the protein. A higher average value of $\tau_c \approx 20$ ns results for the aggregates, as expected for larger particles, but the size distribution of aggregates is of course extremely broad (Fig. 3b). A quantitative interpretation of aggregate anisotropies is additionally complicated by the possible occurrence of several donor chromophores per aggregate (see above), which could result in an apparent decrease of $\langle r \rangle$. Note the much broader width of the r distribution for native molecules, which is presumably dominated by shot noise due to the much smaller number of donor photons emitted at the higher transfer efficiencies. The mean value of r, however, is in good agreement with ensemble donor anisotropy determined for native rhodanese (data not shown).

The donor and acceptor fluorescence lifetimes are depicted in histograms in Fig. 3d and e. While the donor lifetime (Fig. 3d) decreases with increasing transfer efficiency as expected, the acceptor lifetime (Fig. 3e) is not independent of transfer efficiency, suggesting that the molecular environment of the chromophore is significantly different in the two subpopulations. An obvious interpretation would be an additional quenching process caused by the interaction between protein molecules within the aggregates.

In Fig. 5, we show the results from aggregates generated from folded protein at high temperature, not upon refolding from denaturant as above (Fig. 3). The transfer efficiency

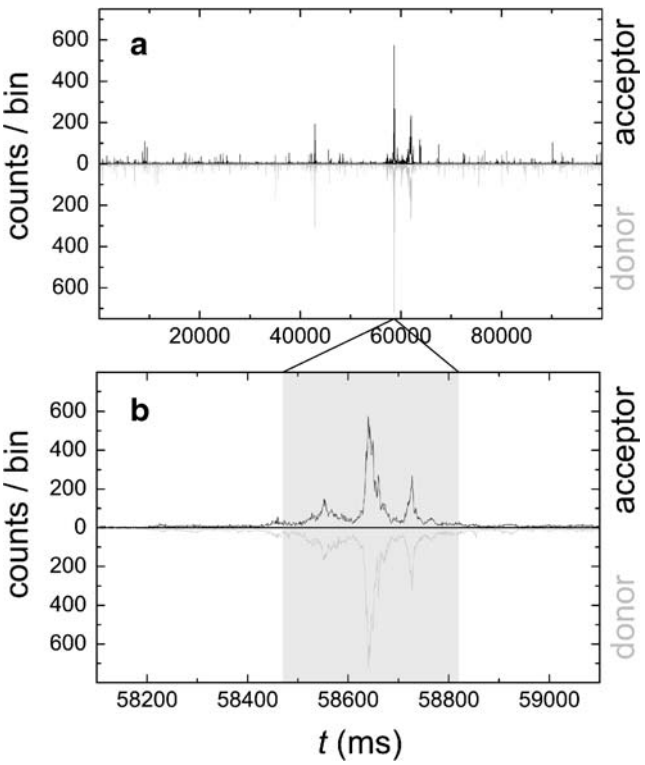

Fig. 4 **a** Representative part of a fluorescence trajectory from the sample described in Fig. 3. The acceptor and donor photon counts per millisecond bin are plotted. The shaded range of the expanded section in **b** represents a single burst of photons originating from one aggregate diffusing through the confocal volume

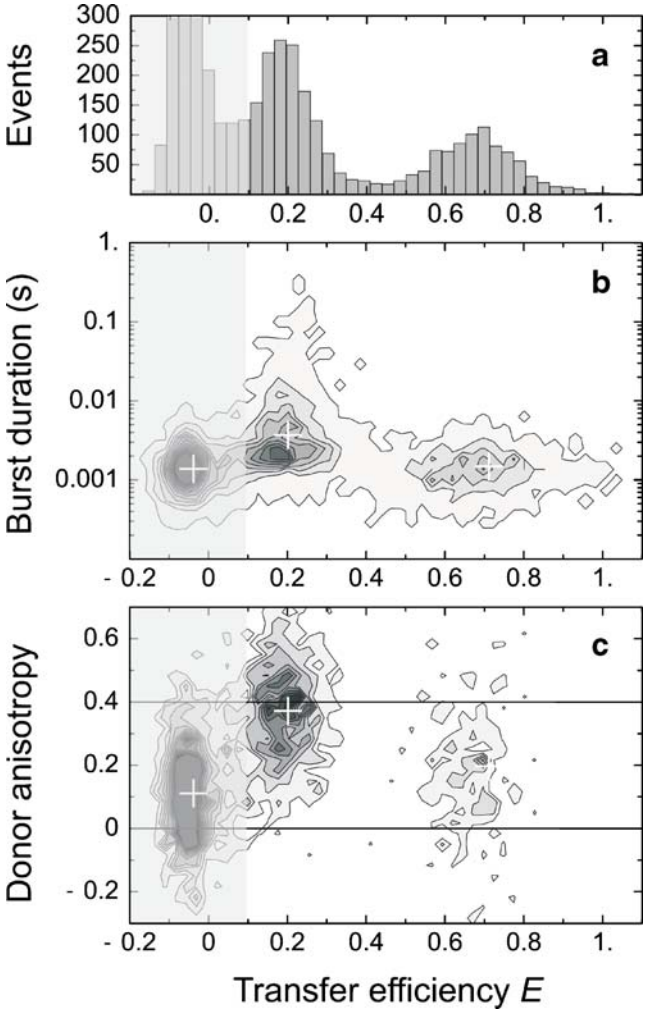

Fig. 5 Multiparameter fluorescence detection analysis of rhodanese aggregates in the presence of native protein. The sample was prepared by heating a 1:1,500 mixture of labeled and unlabeled rhodanese to 50°C for 2.5 min (see "Materials and methods"). Aggregation was stopped by 5-fold dilution on ice yielding a total protein concentration of 300 nM. Data were recorded for 90 min (see "Materials and methods"). **a** FRET efficiency histogram. **b**–**d** Contour plots of two-dimensional histograms calculated from different parameters versus transfer efficiency. *White crosses* mark the respective average value for every subpopulation of events shown in **a**

histogram (Fig. 5a) again exhibits a distinct maximum originating from folded molecules, with its characteristic mean transfer efficiency of 0.70 (see above). However, the aggregate peak shows a decreased transfer efficiency of 0.18 (Fig. 5a) compared to 0.28 in the case of the aggregates generated upon refolding from denaturant (Fig. 3a). Both the increased burst duration (Fig. 5b) and the increased donor anisotropy (Fig. 5c) indicate the presence of a very heterogeneous size distribution, with some bursts approaching diffusion times through the confocal volume of tenths of seconds, similar to our observations for the aggregates generated upon dilution from denaturant (Fig. 3). But the different transfer efficiencies suggest that the two types of aggregates differ in the fine structure of the proteins within the aggregates. These structural differences may indicate that the mechanisms of aggregate formation also differ depending on whether aggregation is initiated from unfolded protein upon dilution of denaturant or from folded protein at high temperature. A possible reason is that the folding and unfolding intermediates of rhodanese, which would be expected to be involved in misfolding and aggregation [35], are not identical. The small differences observed here would usually remain undetected with conventional methods used to study aggregation, most importantly because of the variability in the ratio of folded and misfolded protein. The separation of subpopulations in the single particle approach, however, allows the identification of small changes without interference with the signal from other species present in the same sample.

Even though a detailed interpretation of the difference in transfer efficiencies found for the aggregates generated under different conditions in terms of aggregate structure is beyond the current possibilities, our findings illustrate that single molecule spectroscopy can be used to "fingerprint" different types of aggregates and distinguish them by combining the larger number of observables available from this method compared to techniques such as light scattering or FCS, which have been used heavily to study protein aggregation in the past. Our approach allows the separation of signal from folded and misfolded subpopulations in the same solution, and it can potentially be used to resolve different states of aggregate formation even in substantially more heterogeneous systems than the ones shown here [22]. A promising application are the complex assembly pathways that have been proposed for amyloid formation. This process has so far eluded a comprehensive kinetic and mechanistic description due to the large number of different species that have been suggested to be involved [5, 8, 13, 36]. In favorable cases, distance information obtained from FRET may be useful to constrain molecular models for the structure of proteins within aggregates, especially in cases where the classical structural biology techniques such as X-ray crystallography [6, 7] and nuclear magnetic resonance [37] fail due to the large degree of heterogeneity in the sample. Additional applications may emerge in the field of protein biotechnology, where recombinantly expressed and aggregated proteins are refolded on a large scale to obtain soluble protein, which can then be used for industrial or pharmaceutical purposes. In such processes, the amount of misfolded protein present is often difficult to quantify, and single molecule spectroscopy may be a suitable approach to aid process optimization for proteins that are difficult to refold *in vitro*. Finally, the separation of subpopulations allows the investigation of folding mechanisms even in the

presence of aggregates, which will aid the study of proteins difficult to refold in the absence of molecular chaperones.

Acknowledgements We thank Paul Horowitz for the gift of an expression plasmid for rhodanese and Dominik Hänni for help with taking fluorescence microscopy images of aggregated rhodanese. This work has been supported by the VolkswagenStiftung, the Swiss National Science Foundation and the National Center for Competence in Research for Structural Biology.

References

1. Jaenicke R, Seckler R (1997) Protein misassembly *in vitro*. Adv Protein Chem 50:1–59
2. Tanford C (1968) Protein denaturation. Adv Protein Chem 23:121–282
3. Rudolph R, Lilie H (1996) *In vitro* folding of inclusion body proteins. FASEB J 10(1):49–56 issn: 0892-6638
4. Murphy RM (2002) Peptide aggregation in neurodegenerative disease. Annu Rev Biomed Eng 4:155–174
5. Dobson CM (2003) Protein folding and misfolding. Nature 426 (6968):884–890
6. Nelson R, Eisenberg D (2006) Recent atomic models of amyloid fibril structure. Curr Opin Struct Biol 16(2):260–265
7. Sunde M, Blake C (1997) The structure of amyloid fibrils by electron microscopy and X-ray diffraction. Adv Protein Chem 50:123–159
8. Wetzel R (2006) Kinetics and thermodynamics of amyloid fibril assembly. Acc Chem Res 39(9):671–679
9. LeVine H III (1999) Quantification of beta-sheet amyloid fibril structures with thioflavin T. Methods Enzymol 309:274–284
10. Ban T, Hamada D, Hasegawa K, Naiki H, Goto Y (2003) Direct observation of amyloid fibril growth monitored by thioflavin T fluorescence. J Biol Chem 278(19):16462–16465
11. Goldsbury C, Kistler J, Aebi U, Arvinte T, Cooper GJ (1999) Watching amyloid fibrils grow by time-lapse atomic force microscopy. J Mol Biol 285(1):33–39
12. Gast K, Modler AJ (2005) In: Buchner J, Kiefhaber T (eds) Protein Folding Handbook. Wiley-VCH, Weinheim, pp 673–709
13. Lomakin A, Chung DS, Benedek GB, Kirschner DA, Teplow DB (1996) On the nucleation and growth of amyloid beta-protein fibrils: detection of nuclei and quantitation of rate constants. Proc Natl Acad Sci USA 93(3):1125–1129
14. Modler AJ, Gast K, Lutsch G, Damaschun G (2003) Assembly of amyloid protofibrils via critical oligomers—a novel pathway of amyloid formation. J Mol Biol 325(1):135–148
15. Berland KM, So PTC, Chen Y, Mantulin WW, Gratton E (1996) Scanning two-photon fluctuation correlation spectroscopy: particle counting measurements for detection of molecular aggregation. Biophys J 71:410–420
16. Tjernberg LO, Pramanik A, Bjorling S, Thyberg P, Thyberg J, Nordstedt C, Berndt KD, Terenius L, Rigler R (1999) Amyloid beta-peptide polymerization studied using fluorescence correlation spectroscopy. Chem Biol 6(1):53–62
17. Bark N, Foldes-Papp Z, Rigler R (1999) The incipient stage in thrombin-induced fibrin polymerization detected by FCS at the single molecule level. Biochem Biophys Res Commun 260(1): 35–41
18. Sanchez SA, Chen Y, Muller JD, Gratton E, Hazlett TL (2001) Solution and interface aggregation states of Crotalus atrox venom phospholipase A(2) by two-photon excitation fluorescence correlation spectroscopy. Biochemistry 40(23):6903–6911
19. Sengupta P, Garai K, Balaji J, Periasamy N, Maiti S (2003) Measuring size distribution in highly heterogeneous systems with fluorescence correlation spectroscopy. Biophys J 84(3):1977–1984
20. Bhattacharyya AM, Horowitz PM (2001) The aggregation state of rhodanese during folding influences the ability of GroEL to assist reactivation. J Biol Chem 276(31):28739–28743
21. Horowitz PM, Simon D (1986) The enzyme rhodanese can be reactivated after denaturation in guanidinium chloride. J Biol Chem 261(30):3887–3891
22. Widengren J, Kudryavtsev V, Antonik M, Berger S, Gerken M, Seidel CAM (2006) Single-molecule detection and identification of multiple species by multiparameter fluorescence detection. Anal Chem 78(6):2039–2050
23. Deniz AA, Laurence TA, Beligere GS, Dahan M, Martin AB, Chemla DS, Dawson PE, Schultz PG, Weiss S (2000) Single-molecule protein folding: diffusion fluorescence resonance energy transfer studies of the denaturation of chymotrypsin inhibitor 2. Proc Natl Acad Sci USA 97(10):5179–5184
24. Schuler B (2005) Single-molecule fluorescence spectroscopy of protein folding. ChemPhysChem 6(7):1206–1220
25. Schuler B (2006) In: Bai Y, Nussinov R (eds) Protein folding protocols. Humana, Totowa, New Jersey
26. Schuler B, Lipman EA, Eaton WA (2002) Probing the free-energy surface for protein folding with single-molecule fluorescence spectroscopy. Nature 419(6908):743–747
27. Miller DM, Kurzban GP, Mendoza JA, Chirgwin JM, Hardies SC, Horowitz PM (1992) Recombinant bovine rhodanese: purification and comparison with bovine liver rhodanese. Biochim Biophys Acta 1121(3):286–292
28. Hoffmann A, Kane A, Nettels D, Hertzog D, Baumgärtel P, Lengefeld J, Reichardt G, Horsley DA, Seckler R, Bakajin O, Schuler B (2007) Mapping protein collapse with single molecule fluorescence and kinetic synchrotron radiation circular dichroism spectroscopy. Proc Natl Acad Sci U S A 104(1):105–110
29. Koshioka M, Sasaki K, Masuhara H (1995) Time-dependent fluorescence depolarization analysis in 3-dimensional microspectroscopy. Appl Spectrosc 49(2):224–228
30. Eggeling C, Berger S, Brand L, Fries JR, Schaffer J, Volkmer A, Seidel CA (2001) Data registration and selective single-molecule analysis using multi-parameter fluorescence detection. J Biotechnol 86(3):163–180
31. Ellis RJ (2001) Molecular chaperones: inside and outside the Anfinsen cage. Curr Biol 11(24):R1038–R1040
32. Ploegman JH, Drent G, Kalk KH, Hol WG, Heinrikson RL, Keim P, Weng L, Russell J (1978) The covalent and tertiary structure of bovine liver rhodanese. Nature 273(5658):124–129
33. Alexiev U, Rimke I, Pohlmann T (2003) Elucidation of the nature of the conformational changes of the EF-interhelical loop in bacteriorhodopsin and of the helix VIII on the cytoplasmic surface of bovine rhodopsin: a time-resolved fluorescence depolarization study. J Mol Biol 328(3):705–719
34. Cantor CR, Schimmel PR (1980) Biophysical Chemistry. Freeman, New York
35. Wetzel R (1996) For protein misassembly, it's the "I" decade. Cell 86(5):699–702
36. Wetzel R, Shivaprasad S, Williams AD (2007) Plasticity of amyloid fibrils. Biochemistry 46(1):1–10
37. Tycko R (2006) Amyloid, prions, and other protein aggregates Pt C. Methods Enzymol 413:103–122
38. DeLano WL (2002) The PyMOL Molecular Graphics System. DeLano Scientific, Palo Alto, CA
39. Schuler B, Lipman EA, Steinbach PJ, Kumke M, Eaton WA (2005) Polyproline and the "spectroscopic ruler" revisited with single molecule fluorescence. Proc Natl Acad Sci USA 102: 2754–2759